

Metasurface base on uneven layered fractal elements for ultra-wideband RCS reduction

Cite as: AIP Advances **8**, 035027 (2018); <https://doi.org/10.1063/1.5013106>

Submitted: 10 November 2017 • Accepted: 13 February 2018 • Published Online: 29 March 2018

Jianxun Su,  Yueyang Cui, Zengrui Li, et al.



View Online



Export Citation



CrossMark

ARTICLES YOU MAY BE INTERESTED IN

[Low cost and thin metasurface for ultra wide band and wide angle polarization insensitive radar cross section reduction](#)

Applied Physics Letters **112**, 201601 (2018); <https://doi.org/10.1063/1.5026205>

[Wideband radar cross section reduction using two-dimensional phase gradient metasurfaces](#)

Applied Physics Letters **104**, 221110 (2014); <https://doi.org/10.1063/1.4881935>

[Ultra-wideband RCS reduction and gain enhancement of patterned-surface-based aperture coupling patch antenna with optimized arrangement method](#)

AIP Advances **9**, 075103 (2019); <https://doi.org/10.1063/1.5093216>

Call For Papers!

AIP Advances

SPECIAL TOPIC: Advances in
Low Dimensional and 2D Materials



Metasurface base on uneven layered fractal elements for ultra-wideband RCS reduction

Jianxun Su,¹ Yueyang Cui,¹ Zengrui Li,^{1,a} Yaoqing (Lamar) Yang,²
Yongxing Che,³ and Hongcheng Yin³

¹*College of Information Engineering, Communication University of China,
Beijing 100024, China*

²*Department of Electrical and Computer Engineering, University of Nebraska-Lincoln,
NE 68182, USA*

³*Science and Technology on Electromagnetic Scattering Laboratory, Beijing 100854, China*

(Received 10 November 2017; accepted 13 February 2018; published online 29 March 2018)

A novel metasurface based on uneven layered fractal elements is designed and fabricated for ultra-wideband radar cross section (RCS) reduction in this paper. The proposed metasurface consists of two fractal subwavelength elements with different layer thickness. The reflection phase difference of 180° ($\pm 37^\circ$) between two unit cells covers an ultra-wide frequency range. Ultra-wideband RCS reduction results from the phase cancellation between two local waves produced by these two unit cells. The diffuse scattering of electromagnetic (EM) waves is caused by the randomized phase distribution, leading to a low monostatic and bistatic RCS simultaneously. This metasurface can achieve -10dB RCS reduction in an ultra-wide frequency range from 6.6 to 23.9 GHz with a ratio bandwidth (f_H/f_L) of 3.62:1 under normal incidences for both x- and y-polarized waves. Both the simulation and the measurement results are consistent to verify this excellent RCS reduction performance of the proposed metasurface. © 2018 Author(s). All article content, except where otherwise noted, is licensed under a Creative Commons Attribution (CC BY) license (<http://creativecommons.org/licenses/by/4.0/>). <https://doi.org/10.1063/1.5013106>

I. INTRODUCTION

With the rapid development of the contemporary radio technology and the military electronic technology, the ability of the combat defence systems search and track the target have been enhanced at a great extent.¹ There are many researches focus on the achievement of electromagnetic (EM) transparency or invisibility of the target in recent years. Radar cross section (RCS) as an important physical quantity is used to characterize the electromagnetic scattering properties of the target. To reduce the RCS effectively of the target is a challenging objective for the electromagnetic researchers. Different techniques have been proposed in the previous literatures to reduce the RCS, such as applying radar absorbing materials (RAM) which transforms the electromagnetic energy into heat,² however the RAM often operate in the vicinity of the resonance frequency. Another technique is altering the appearance of the target (Shaping) to redirect the scattered field to more directions, but that increases the complexity of the design.³

Metamaterials are artificial structures which capability of manipulating the electromagnetic waves to obtain unusual properties, such as negative refraction,⁴ subwavelength focusing,⁵ and electromagnetic invisibility cloaking.⁶ Metasurface, as a new kinds of ultra-thin metamaterials that consist of a monolayer of planar metallic structure, provides an unique way of manipulating the EM waves and achieves the excellent RCS reduction of metallic targets. Generally, phase cancellation is utilized to achieve RCS reduction. The basic idea is to exploit the cancellation effects arising from the well-known 180° phase difference between the corresponding reflection coefficients. The scattered energy could be redirected away from the source direction. A planar structure based on a combination

^aCorrespondence and requests for materials should be addressed to Zengrui Li (email: zrli@cuc.edu.cn)

of perfect electric conductor (PEC) and artificial magnetic conductor (AMC) in a chessboard-like metasurface is proposed in Ref. 7. But due to the narrow reflection in-phase bandwidth of the AMC, the RCS reduction frequency range is limited. In Ref. 8, a 10 dB RCS reduction more than 40% frequency bandwidth is obtained by using two AMC unit cells based on Jerusalem Cross configuration. In 2015, C. A. Balanis et al.⁹ proposed a hexagonal checkerboard surface of periodic phase arrangement, with the -10 dB monostatic RCS reduction bandwidth of about 61%. A chessboard metasurface which consists of four E-shaped and saltire arrow unit cells can achieve a frequency bandwidth of 85% for 10 dB RCS reduction in 2016,¹⁰ then Su proposed a metasurface based on a symmetric split ring and a cut wire, the RCS is suppressed by 10 dB from 7.9 to 20.8 GHz.¹¹ Moreover, in Ref. 12 a frequency bandwidth of 84.7% with 10 dB RCS reduction is obtained. A kind of polarization rotation reflection surface (PRCS) based on the unit cell consists of a square and L-shaped patches is applied to achieve a 10 dB reduction over frequency bandwidth of 98%.¹³ A chessboard-like metasurface is designed and fabricated in Ref. 14, by applying a binary optimization algorithm and linking it to a full-wave simulation package, it works over an ultra-wide band of frequency from 3.8 to 10.7 GHz. In addition, Ref. 15 proposed a coding phase gradient metasurface (CPGM) made of the N-shape metallic pattern, which could come true 10 dB RCS reduction in frequency bands of 7.8-13.5 GHz with a radio bandwidth of 1.95:1. To meet the needs of engineering applications, it is highly desirable to design a metasurface for reducing monostatic and bistatic RCS of the object over an ultra-wide frequency band.

In this article, two kinds of Minkowski fractal structures are chosen as the basic unit cells to compose the proposed chessboard metasurface. Through design precisely this two unit cells to obtain their reflection phase difference of $180^\circ \pm 37^\circ$. The proposed metasurface realizes a more than 10 dB RCS reduction in an ultra-wide frequency band from 6.6 to 23.9 GHz with a bandwidth of 113% (ratio bandwidth of 3.62:1) for both polarizations. In addition, the array theory and particle swarm optimization (PSO) algorithm are utilized to optimize and obtain phase layout for diffusion scattering of EM waves under x- and y-polarized normal incidence. The simulated and the measured results validate effectively the capacity of the proposed metasurface for reducing the monostatic and bistatic RCS of the target and significantly extending frequency bandwidth.

II. OPTIMIZED METASURFACE DESIGN

A. Unit cell designs

Minkowski Fractal element is chosen as the basic unit cell of the proposed metasurface on account of its fractal geometry with an excellent self-similar property, which is useful for adjusting the unit cell size and broadening the working bandwidth, in addition, the simple design and the easy fabrication. This paper uses two kinds of Minkowski fractal elements, one is patch structure, and the other is ring structure. The basic unit cell is constituted of two metallic layers which are separated by a F4B substrate plate with dielectric constant of 2.65 and loss tangent of 0.001. Fig. 1 shows the 3D modeling, as well as, the top view and side view of two fractal elements.

The parameters of the unit cell A and B are also shown in Fig. 1. The bottom layer is metallic plate. In a certain frequency band, the reflection phase of the basic unit cell is influenced by its geometrical parameters. In our simulation, the substrate thickness $h1$ and $h2$ change in 2, 4, 6 mm, meanwhile, the side length $L1$ varies from 0.8 to 7.8 mm and the side length $L2$ varies from 1.6 to 7.9 mm both with the step size of 0.1 mm. While the other dimensions are fixed as follows: the periodicity of the unit cell is $P=8$ mm, the width is $w=0.3$ mm, the inside length is $L_{in}=1.5$ mm and gap is $g=0.7$ mm. These two kinds of unit cells are independently simulated by frequency domain solver with periodic boundary condition (PBC) of CST microwave studio to obtain the reflection phase.

For a dual checkerboard metasurface the RCS reduction can be approximated by

$$\text{RCS reduction} = 10 \log \left[\frac{A_1 e^{jP_1} + A_2 e^{jP_2}}{2} \right]^2 \quad (1)$$

where A_1 and A_2 are the reflection coefficient amplitudes of two unit cells, and P_1 and P_2 are their reflection phase. According to this formula, more than 10 dB RCS reduction can be achieved

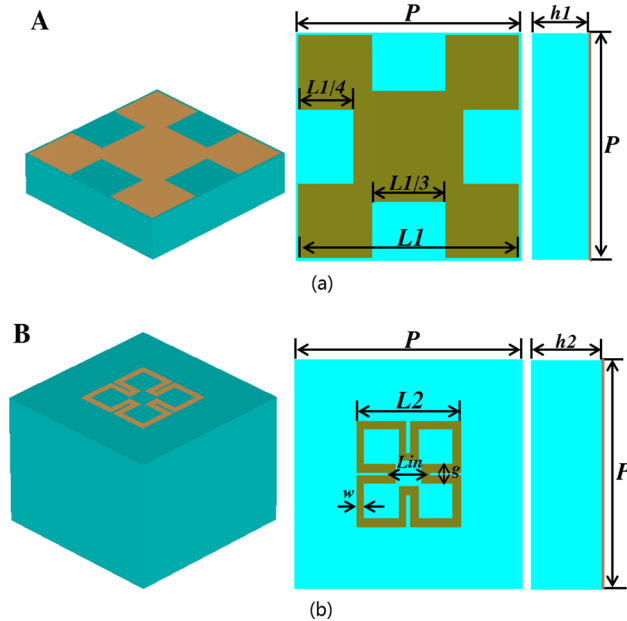


FIG. 1. 3D modeling and geometry of the basic unit cells. (a) the unit cell A (b) the unit cell B.

when phase difference of two basic unit cells is between $180^\circ \pm 37^\circ$. Hence, after the simulation, we use a MATLAB program to look for two unit cells with $180^\circ \pm 37^\circ$ phase difference in the largest possible frequency band. The job of this program is to compare the frequency bandwidth of any two different unit cells with a $180^\circ \pm 37^\circ$ reflection phase difference. This searching process results in the optimal parameters of two basic unit cells, which are $h1=2$, $L1=7.8$ and $h2=6$, $L2=3.7$ mm, respectively. The reflection phase curves versus frequency of these two unit cells as well as their reflection phase difference are described in Fig. 2. A clear find from the curves, the reflection phase difference ($180^\circ \pm 37^\circ$) stays in the frequency range from 6.41 to 22.79 GHz. Compared with previous researches, the frequency bandwidth can be extended effectively by the Minkowski fractal element. In other words, two selected unit cells can be used in a chessboard configuration to achieve a low-scattering property in ultra-wide frequency band.

B. Metasurface design

In order to satisfy the periodic boundary condition (PBC) used in simulation, a lattice contains 8×8 identical unit cells. The proposed metasurface constituted of 4×4 lattices. The geometry structure

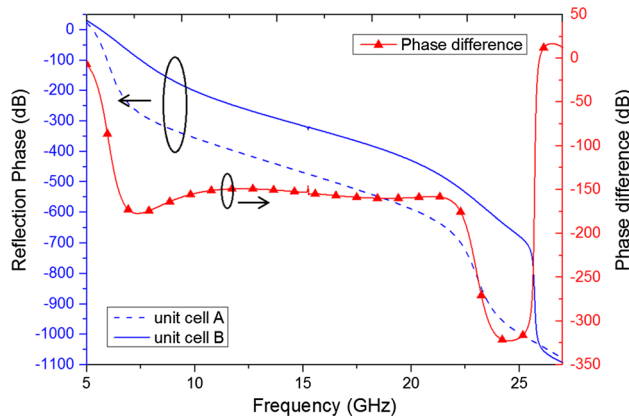


FIG. 2. Reflection phase of two unit cells and phase difference between them.

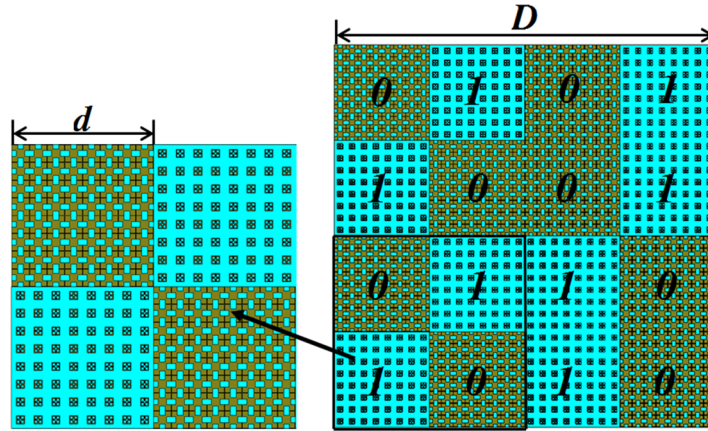


FIG. 3. Geometry structure of the proposed metasurface.

is shown in Fig. 3. The dimension of the lattice and the metasurface is $d=64$ and $D=256$ mm, respectively. The proposed metamaterials are comprised of digital elements and are controlled by the coding sequences of them.¹⁶ In binary case the phase difference is 180° , therefore for 1-bit coding metamaterials, artificially regulate “0” element with a 0° phase response and “1” element with a 180° phase response. In this article, the unit cell A and B are denominated as “0” and “1” binary digital elements, respectively.

Once the lattice has been prepared, we are going to search for the optimal layout of the metasurface. The simplest way is to create a random phase distribution matrix.¹⁷ But it cannot guarantee an optimal result, and the continuous phase of change is difficult to achieve in reality. Hence, we adopt a comprehensive approach combining array theory, coding matrix and optimization algorithm to solve this issue. Considering the array of $M \times N$ lattices of opposite reflection phase (0° and 180°), according to the array theory, the scattering field of the metasurface can be expressed as

$$E^S(\theta, \varphi) = EF(\theta, \varphi) \cdot AF(\theta, \varphi) \quad (2)$$

where θ and φ are the elevation and azimuth angles, respectively. EF and AF are the pattern function of a lattice and the array factor, respectively. Here, the EF is fixed and the AF is expressed by

$$AF(\theta, \varphi) = \sum_{m=1}^M \sum_{n=1}^N \exp \left\{ -j \left[2\pi \sin\theta (\cos\varphi \cdot md_x + \sin\varphi \cdot nd_y) / \lambda + \Phi(m, n) \right] \right\} \quad (3)$$

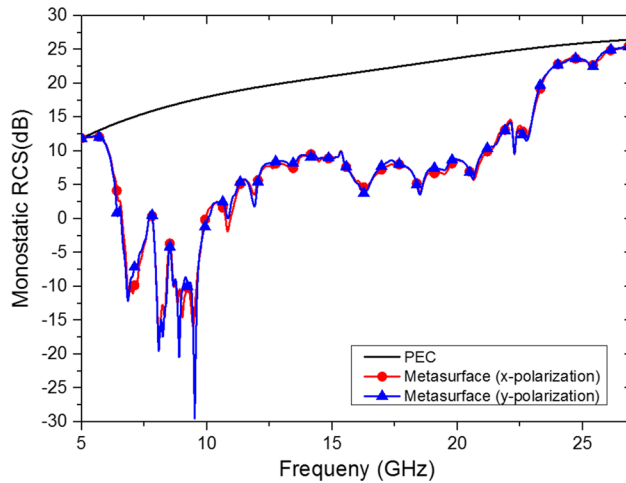


FIG. 4. The simulated monostatic RCS of the proposed coding metasurface and the equal-sized PEC surface under x- and y-polarized incident waves.

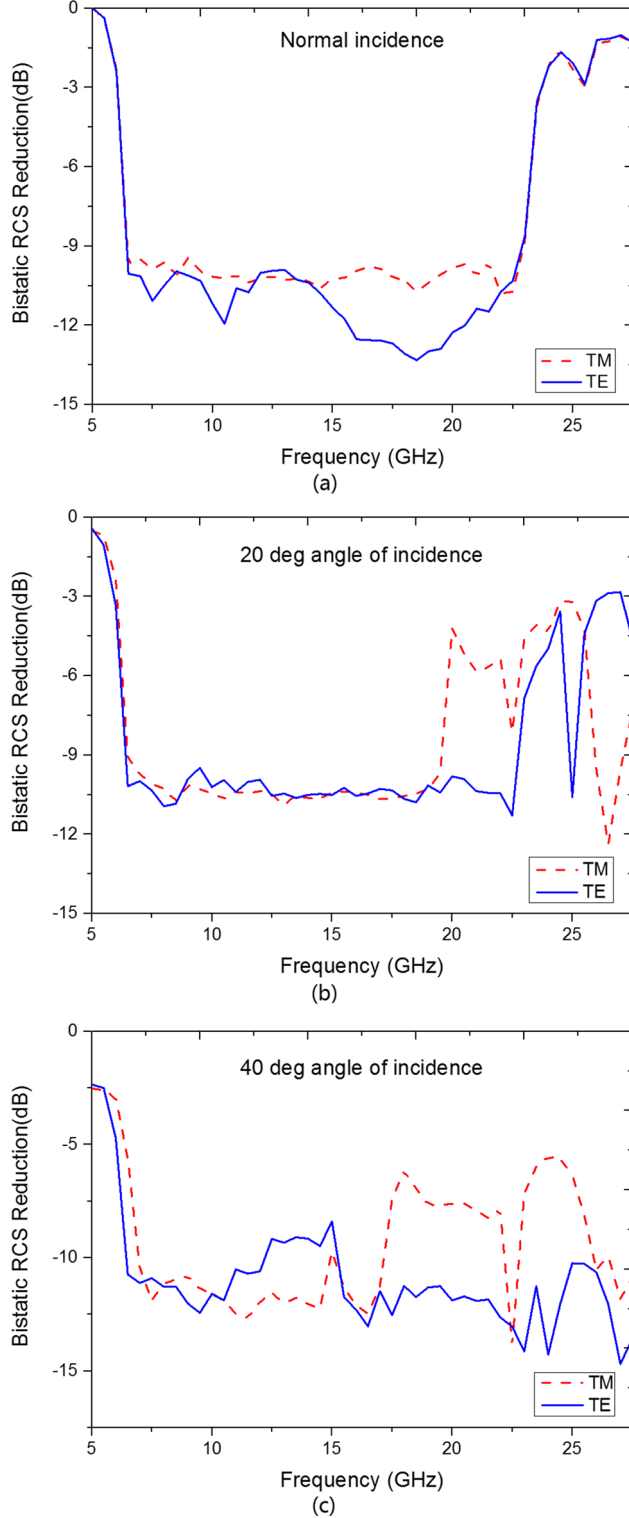


FIG. 5. The bistatic RCS reduction of the metasurface versus frequency at different angles of incidence. (a) Normal incidence. (b) 20 degrees angle of incidence. (c) 40 degrees angle of incidence.

The lattices are uniformly spaced with d_x in the x direction and d_y in the y direction. $\theta(m, n)$ is the initial phase of the lattice. To realize EM wave diffusion on a planar metasurface, we propose a scheme so that all the digital elements of the metasurface are randomly arranged to achieve the

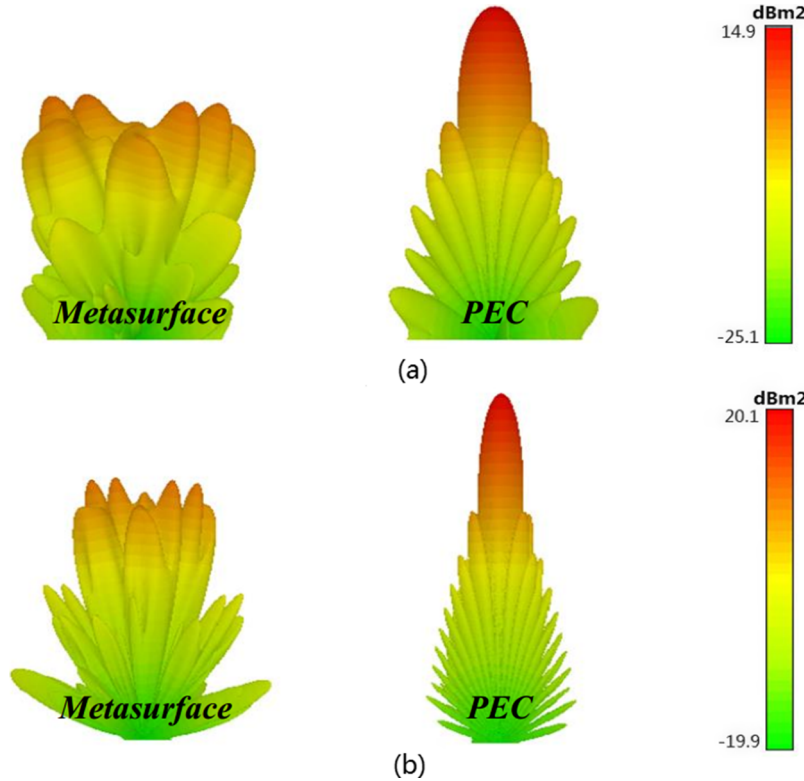


FIG. 6. The 3-D plots of the simulated scattering pattern of the proposed metasurface and the equal-sized PEC surface at (a) 7 GHz (b) 13 GHz.

desired diverse scattering pattern. In this scheme, a particle-swarm optimization (PSO) algorithm is employed to find the optimal arrangement of the digital elements. During the optimization, a far-field pattern prediction algorithm is used as an auxiliary module to save the effort required for tremendous full-wave simulations.^{18,19} Fig. 3 shows the optimal phase layout, which could redirect the scattering energy to more directions under normal incidence.

III. SIMULATED AND MEASURED RESULTS

A. Simulated result

To corroborate the physical phenomena above-mentioned, as well as, the RCS reduction and diffusion effects of the proposed metasurface, the transient solver of CST Microwave Studio is used to full-wave simulate the full structure under normal incidence with x- and y-polarizations. An equal-sized perfect electric conductor (PEC) surface is simulated as the reference. Fig. 4 shows the simulated monostatic RCS of the proposed metasurface and the reference PEC surface. A larger than 10 dB RCS reduction is achieved over the ultra-wide frequency ranges from 6.4 to 23 GHz (112.8% bandwidth). It is worth noting that the RCS reduction bandwidth is in accordance with the results predicted by the reflection phase difference features between two fractal basic unit cells as shows in Fig. 2. Due to the symmetry, the phase response of the lattice is the same for both polarizations. Thus the RCS reduction of the proposed metasurface is polarization independence.

In the previous section, an optimal layout of the metasurface is obtained, it is done because of more sidelobes will be increased and the EM energy is redirected to more direction. The bistatic RCS reduction is defined by

$$\text{Bistatic RCS Reduction} = \frac{\text{Max (Bistatic RCS of metasurface)}}{\text{Max (Bistatic RCS of equal-sized metal)}} \quad (4)$$

where the $\text{Max}(\dots)$ function domain covers the bistatic scattering angles (θ_s and φ_s) which covers the upper half-space of the metasurface ($0 \leq \theta_s \leq 0.5\pi$ and $0 \leq \varphi_s \leq 2\pi$). The bistatic RCS reduction at different incident angles versus frequency for both TM and TE-polarization is shown in Fig. 5. From the figures, it is found that the excellent bistatic RCS reduction when the angle of incidence changes and the bistatic RCS reduction of the proposed metasurface is also polarization independence.

To further illustrate the performance of the proposed metasurface, the comparison of the simulated 3D bistatic scattering patterns of the proposed metasurface and the equal-sized PEC surface for normal incidence at 7 and 13 GHz are illustrated in Fig. 6. The maximum bistatic RCS value is reduced by 9.6 and 10.2 dB at 7 and 13 GHz, respectively. The proposed metasurface generates diffusion scattering instead of the peak scattering of the reference PEC surface. According to the law of energy conservation, the maximum of scattered field is suppressed at a low level, leading to a low bistatic RCS.

To investigate the scattering profiles of the proposed metasurface under oblique incidences, we considered four incident angles ($\theta^{in} = 15^\circ, 20^\circ, 30^\circ, 40^\circ$) for both transverse-electric (TE) and transverse-magnetic (TM) polarizations in this simulation. Figs. 7(a) and (b) show the simulated RCS reduction of the metasurface over a broad frequency band at the incidence angles considered. From these figures, we can see clearly that in the case of TM-polarization, the metasurface works well

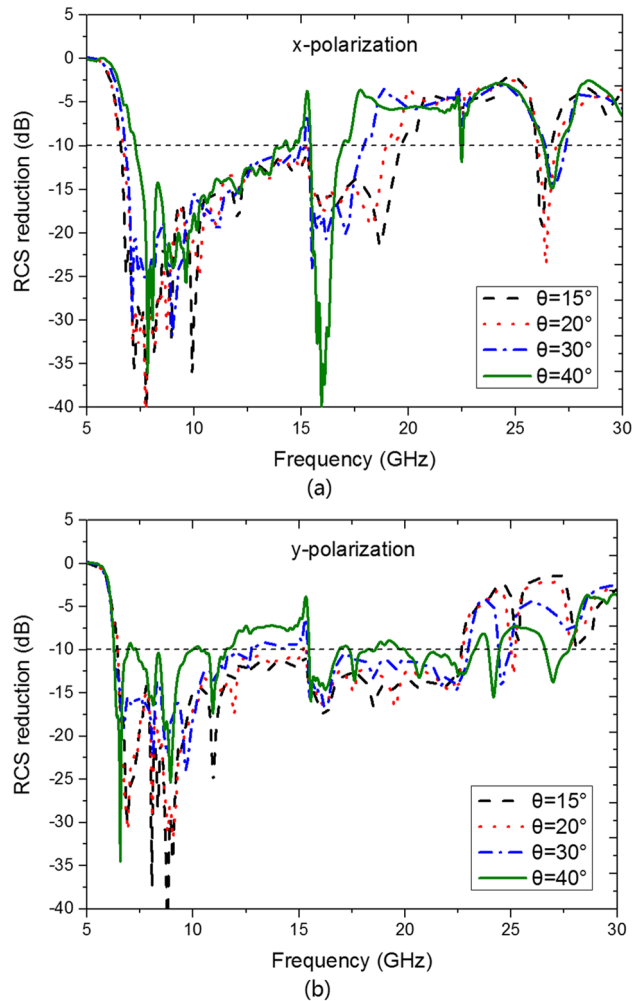


FIG. 7. Simulation results of the metasurface under the oblique incidences for (a) TE-polarization (b) TM-polarization. TE/TM: The direction of the electric/magnetic field is perpendicular to the plane of incidence.

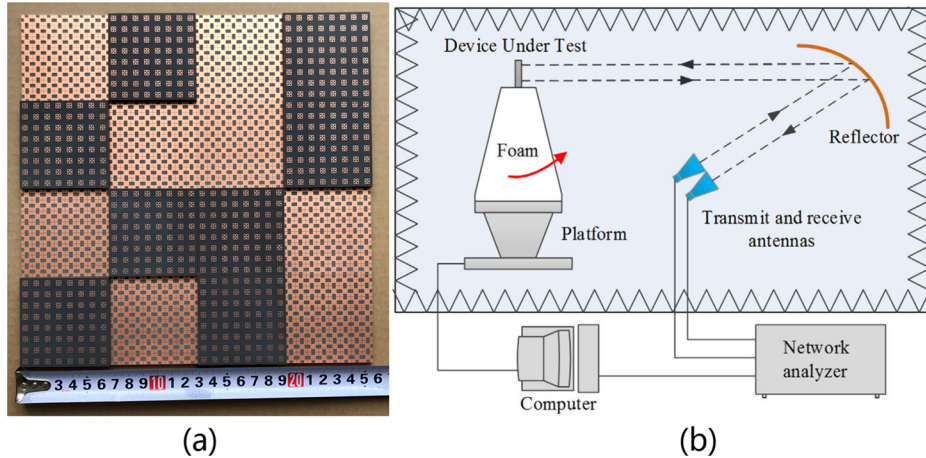


FIG. 8. Monostatic RCS measurement (a) The fabricated metasurface (b) Schematic view of the compact range system.

for a wide range of incident angles, however, the operation bandwidth of the metamaterial decreased as the incident angle increased for TE-polarization. At the same time, we notice this phenomenon also appears in the other designs reported in the literature.^{20–22} It means that the high sensitivity to the incident angle for TE-polarization is not only a challenge for our design but also the objective in our future work.

B. Measured result

In order to confirm the theoretical results and the validity of the simulation, a sample of the proposed metasurface with a total dimensions $256 \times 256 \text{ mm}^2$ is fabricated and measured. The sample is manufactured by LPKF ProtoLaser with printed circuit board (PCB) technology, is depicted in Fig. 8(a). Because the dielectric layer of the proposed metasurface is uneven, these 16 lattices are fabricated independently and we paste them on a metal plate according to the phase arrangement, as shown in Fig. 3. The monostatic RCS is measured by compact range system of *National Electromagnetic Scattering Laboratory* in Beijing. The measurement setup is shown in Fig. 8(b). For the monostatic RCS reduction measurement, two identical horn antennas are used as transmitting and receiving devices. The spherical waves emitted by the horn antenna are reflected

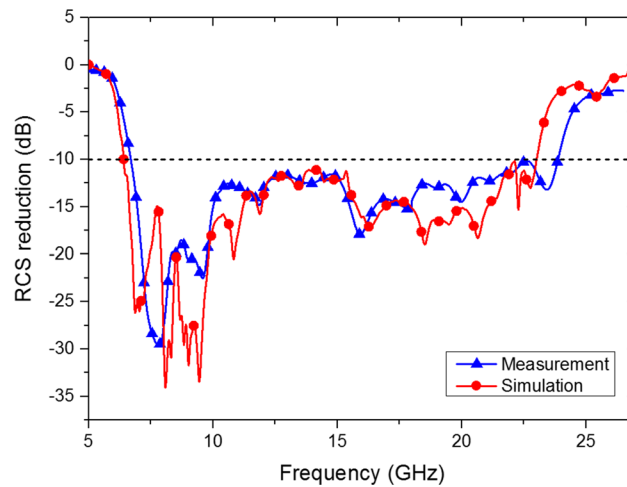


FIG. 9. The simulated and measured monostatic RCS reduction of the proposed coding metasurface under x-polarized normal incident.

TABLE I. Comparisons between the results of this work and earlier checkerboard surfaces. RCSR: Radar Cross Section (RCS) Reduction, FR: Frequency range, BW: The relative bandwidth ($BW = (f_H - f_L)/f_c$, $f_c = (f_H + f_L)/2$), RBW: The ratio bandwidth ($RBW = f_H/f_L$).

	RCSR (<=dB)	FR (GHz)	BW (%)	RBW
8	-10	14.5-21.8	40.2	1.50
9	-10	4.2-7.9	61	1.88
10	-10	9.4-23.3	85	2.47
11	-10	7.9-20.8	89.9	2.63
12	-10	17-42	84.7	2.47
13	-10	6.1-17.8	98	2.91
15	-10	3.8-10.7	95	2.81
16	-10	9.83-19.12	64.2	1.95
This work	-10	6.6-23.9	113	3.62

by the parabolic metal reflector and become a plane wave. Short test distance between metasurface sample and reflector is easy to meet the far field conditions. Then, the scattering performance is evaluated by the transmission coefficients obtained by vector network analyzer. The measured monostatic RCS reduction curve versus frequency under x-polarized normal incidence is shown in Fig. 9. A larger than 10 dB monostatic RCS is obtained over an ultra-wide frequency band from 6.6 to 23.9 GHz with a ratio bandwidth of 3.62:1. The measured result agrees well with the simulation result. Slight frequency deviation can be attributed to fabrication and measurement error. Moreover, Table I shows the comparison between the previous researches and this work. Through the comparison of available results, the RCS reduction bandwidth is extended significantly by our proposed metasurface. Overall, the excellent performance of the proposed metasurface is verified.

IV. CONCLUSION

A novel metasurface based on uneven layered fractal elements is designed, fabricated and measured for ultra-bandwidth RCS reduction. The proposed metasurface consists of two kinds of Minkowski fractal elements, one is patch and the other is ring structure. The $180^\circ \pm 37^\circ$ reflection phase difference between this two unit cells that realizes a more than 10 dB RCS reduction from 6.6 to 23.6 GHz (113% frequency bandwidth). The particle swarm optimization (PSO) algorithm combining with the array theory are utilized to optimize the coding matrix of digital elements and obtain the optimal layout for diffusion scattering under normal incidence, leading to an excellent bistatic RCS reduction. The measurement and simulation results are consistent to verify the ultra-bandwidth diffusion scattering and RCS reduction performance of the proposed metasurface for both polarizations.

ACKNOWLEDGMENTS

This work was supported by the National Natural Science Foundation of China (61671415 and 61701448), and the key projects of engineering planning of Communication University of China (3132016XNG1604).

¹ G. T. Ruck, D. E. Bamck, W. D. Stuart *et al.*, Plenum, 2, New York, NY, USA, 1970.

² M. Yoo, H. K. Kim, and S. Lim, *IEEE Antennas Wireless Propagat.* **15**, 414–417 (2016).

³ E. F. Knott, M. T. Tuley, and J. F. Shaeffer, *Radar Cross Section*, 2nd ed. (Artech House, Norwood, MA, USA, 1993), p. 269.

⁴ H. J. Lezec, J. A. Dionne, and H. A. Atwater, *Science* **316**, 430 (2007).

⁵ K. Kitamura, K. Sakai, and S. Noda, *Optics Express* **18**, 4518 (2010).

⁶ D. Schurig *et al.*, “Metamaterial electromagnetic cloak at microwave frequencies,” *Science* **314**, 977 (2006).

⁷ M. Paquay, J. C. Iriarte, I. Ederra, R. Gonzalo, and P. D. Maagt, *IEEE Trans. Antennas Propagat.* **55**, 3630 (2007).

⁸ J. C. I. Galarregui, A. T. Pereda, J. L. M. D. Falcón *et al.*, *IEEE Trans. Antennas Propagat.* **61**, 6136 (2013).

⁹ W. Chen, C. A. Balanis, and C. R. Birtcher, *IEEE Trans. Antennas Propagat.* **63**, 2636 (2015).

¹⁰ S. H. Esmaeli and S. H. Sedighy, *Electron. Lett.* **52**, 70 (2016).

- ¹¹ P. Su, Y. Zhao, S. Jia, W. Shi, H. Wang *et al.*, *Sci. Rep.* **6**, 1 (2016).
- ¹² H. Sun, C. Gu, X. Chen *et al.*, *Sci. Rep.* **7**, 1 (2017).
- ¹³ Y. Jia, Y. Liu, Y. J. Guo *et al.*, *IEEE Trans. Antennas Propagat.* **65**, 3291 (2017).
- ¹⁴ M. J. Hajji-Ahmadi, V. Nayyeri, M. Soleimani, and O. M. Ramahi, *Sci. Rep.* **7**, 11437 (2017).
- ¹⁵ Q. Q. Zheng, Y. F. Li, J. Q. Zhang, H. Ma, J. F. Wang, Y. Q. Pang, Y. J. Han, S. Sui, Y. Shen, H. Y. Chen, and S. B. Qu, *Sci. Rep.* **7**, 43543 (2017).
- ¹⁶ T. J. Cui, M. Q. Qi, X. Wan, J. Zhao, and Q. Cheng, *Sci & Appl* (2014).
- ¹⁷ L. H. Gao, Q. Cheng, J. Yang, S. J. Ma *et al.*, *L. Sci. & Appl.* **4**, 324 (2015).
- ¹⁸ J. X. Su, Y. Lu, Z. Y. Zheng *et al.*, *J. Appl. Phys.* **120**, 205107 (2016).
- ¹⁹ J. X. Su, Y. Lu, H. Zhang *et al.*, *Sci. Rep.* **7**, 42283 (2017).
- ²⁰ A. Edalati and K. Sarabandi, *IEEE Trans. Ant. & Prop.* **62**, 747 (2014).
- ²¹ W. Chen, C. A. Balanis, and C. R. Birtcher, *IEEE Trans. Ant. & Prop.* **63**, 2636 (2015).
- ²² W. Chen, C. A. Balanis, and C. R. Birtcher, *IEEE Trans. Ant. & Prop.* **64**, 4133 (2016).